CXCL9 is a dual-role biomarker in colorectal cancer linked to mitophagy and modulated by ALKBH5

GENG HU[1], SHIJUN SHEN[2] and MINGCHAO ZHU[3]

[1]Department of Laboratory, Geriatric Hospital Affiliated to Wuhan University of Science and Technology, Wuhan, Hubei 430081, P.R. China; [2]Department of Hepatobiliary and Pancreatic Minimally Invasive Surgery, Lincang People's Hospital, Lincang, Yunnan 677099, P.R. China; [3]Department of Laboratory, Tianmen First People's Hospital, Tianmen, Hubei 431700, P.R. China

Received October 17, 2024; Accepted March 18, 2025

DOI: 10.3892/mmr.2025.13553

Abstract. Colorectal cancer (CRC), the third most prevalent cancer globally, shows a diminished 5-year survival rate compared with patients at early stages of the disease, underscoring the urgency for early diagnostic biomarker identification. The C-X-C motif chemokine ligand (CXCL) family plays a significant role in immune modulation and cancer progression. the present study constructed a prognostic model for CXCL family in CRC and conducted an in-depth investigation of the hub gene CXCL9 within the model. CXCL9 is highly expressed in CRC while high expression levels of CXCL9 in patients with CRC often indicates an improved prognosis. Through Gene Ontology, Kyoto Encyclopedia of Genes and Genomes and gene set enrichment analysis enrichment analysis, it was discovered that CXCL9 is not only associated with immune modulation but also closely related to pathways that affect the occurrence and development of cancer. CXCL9 is closely related to mitophagy and blocks autophagy flow by altering the expression of autophagy-related genes. Additionally, it was found that CXCL9 is a downstream gene modified by ALKBH5 and can partially restore the tumor-suppressive effects induced by the knockdown of ALKBH5. These studies indicated that CXCL9 is a prognostic marker in CRC and plays a dual role in cancer progression: It activates immune responses on one hand and promotes the malignant characteristics of cancer on the other hand.

Introduction

Colorectal cancer (CRC) is the third most common cancer, with significant health implications worldwide (1). The 5-year survival rate for patients with CRC is ~90% when diagnosed at early and localized stages. However, this rate decreases markedly to only 13.1% for those diagnosed at later, metastatic stages (2). Currently, the treatment of colorectal cancer includes various approaches such as surgical resection, chemotherapy, radiotherapy, targeted therapy, and immunotherapy. Surgery is the primary treatment, with curative intent for early-stage patients (3,4). Combined surgery and chemoradiotherapy are often used for metastatic disease, but complications and side effects can be severe (5-9). To mitigate these challenges, complementary approaches such as traditional Chinese herbal medicines have been used in combination therapies to reduce the adverse reactions of radiotherapy and chemotherapy, thereby improving the quality of life for patients (10). Targeted therapies, such as anti-VEGF and anti-EGFR drugs, have shown efficacy in improving survival with fewer side effects compared to traditional treatments. However, issues such as off-target effects and drug resistance remain significant challenges (11,12). Immunotherapy, particularly anti-programmed cell death 1 (PD-1) and anti-cytotoxic T lymphocyte associated protein 4 agents, has achieved remarkable success in colorectal cancer with high microsatellite instability and mismatch-repair deficiency (MSI-H/dMMR) but has limited effectiveness in patients with microsatellite stable and proficient mismatch repair (MSS/pMMR) (13-16). Overall, while progress has been made in treating CRC, several challenges remain. Further research into the disease mechanisms and the development of new therapeutic targets and strategies are needed to improve patient outcomes and quality of life.

The C-X-C motif chemokine ligand (CXCL) family plays a crucial role in a variety of biological processes, including cell migration, tumor development, angiogenesis, and several other essential functions (17). These chemokines are instrumental in the recruitment and activation of immune cells such as neutrophils, monocytes, T-lymphocytes and natural killer cells. They serve roles in both inflammatory and homeostatic functions; inflammatory chemokines such as CXCL8 are involved in directing leukocytes to sites of infection or injury, whereas homeostatic chemokines such as CXCL12 maintain the baseline migration of immune cells and are consistently expressed (18). CXCL9, a member of the CXC chemokine family, plays a multifaceted role in the tumor microenvironment. Expressed predominantly by tumor-associated macrophages and dendritic

Correspondence to: Dr Geng Hu, Department of Laboratory, Geriatric Hospital Affiliated to Wuhan University of Science and Technology, 2 Huangjiahu West Road, Wuhan, Hubei 430081, P.R. China
E-mail: m13657128805_2@163.com

Key words: C-X-C motif chemokine ligand 9, biomarker, mitophagy, m6a, colorectal cancer

cells (DCs), CXCL9 is instrumental in modulating antitumor immunity (19). It is particularly noted for its involvement in the recruitment and positioning of CXCR3-expressing stem-like CD8 T cells, which are crucial for responses to anti-PD(L)-1 treatment (20-22).

Previous studies have highlighted the diverse roles of CXCL9 across various cancer types. For instance, in breast cancer, CXCL9 has been shown to promote tumor progression by enhancing the recruitment of immune cells and modulating the tumor microenvironment (23-26). In melanoma, CXCL9 expression has been associated with improved response to immunotherapy, suggesting its potential as a predictive biomarker (27,28). In lung cancer, CXCL9 has been implicated in both tumor suppression and progression (29,30). These findings underscore the complexity of CXCL9's function and its potential as a therapeutic target in multiple cancers.

Although the CXCL family is commonly associated with promoting anti-tumour responses, there are a number of findings demonstrating pro-oncogenic effects of the CXCL family, suggesting a more complex role in tumour progression. In order to understand the molecular function of CXCL9 in colorectal cancer, the present study conducted bioinformatics analysis and *in vitro* validation.

Materials and methods

Data acquisition. The Cancer Genome Atlas (TCGA) database (https://www.cancer.gov/tcga) and the Gene Expression Omnibus (GEO) repository (https://www.ncbi.nlm.nih.gov/geo/) were used to obtain gene expression data. To obtain comprehensive gene expression data, the present study used two major public databases: The Cancer Genome Atlas (TCGA; https://www.cancer.gov/tcga) and the Gene Expression Omnibus (GEO; https://www.ncbi.nlm.nih.gov/geo/). TCGA is a landmark cancer genomics program that has characterized over 20,000 primary cancer and matched normal samples across 33 cancer types. The present study specifically used the TCGA dataset for colorectal adenocarcinoma (COAD), which provides rich genomic and transcriptomic information, enabling the exploration of the molecular underpinnings of colorectal cancer. Additionally, the present study focused on the GSE41258 dataset from GEO, which includes samples from patients with colonic neoplasms treated at Memorial Sloan-Kettering Cancer Center between 1992 and 2004. This dataset comprises 390 expression arrays from primary colon adenocarcinomas, adenomas, metastases, and corresponding normal mucosae. Data processing was performed using R (version 4.4.1, http://www.R-project.org/).

Definition of the CXCL family prognostic model. Least absolute shrinkage and selection operator (LASSO) regression was used to create a prognostic signature using the samples from the TCGA cohort. The regression coefficients (β) from the CXCL family model were then combined with the relevant gene expression levels to generate a multi-gene marker-based predictive risk score. The TCGA data was used to train the risk score model, which was built as follows: Risk score=expression level of CXCL1 x (-0.097330812) + expression level of CXCL6 x (0.08298018) + expression level of CXCL8 x (0.009198228) + expression level of CXCL9 x (-0.053426341) + expression level of CXCL11 x (-0.10920036) + expression level of CXCL12 x (0.051584401) + expression level of CXCL14 x (-0.055678695). LASSO regression was implemented with the glmnet package (version 4.1.2; https://CRAN.R-project.org/package=glmnet). Cross-validation and model evaluation were carried out using the ROCR package (version 1.0.11; https://CRAN.R-project.org/package=ROCR). ggplot2 (version 3.3.6; https://CRAN.R-project.org/package=ggplot2) was used for data visualization.

Construction of protein-protein interaction (PPI) networks. Using the STRING database, a PPI network map was constructed encompassing the CXCL family and their interacting proteins. The network was subsequently refined and visualized within the Cytoscape (version 3.9.1; http://cytoscape.org/download) (31). Hub genes were identified employing the Degree algorithm (32), where the size, color, and spatial arrangement of the nodes within the network corresponded to their respective Degree scores.

Survival analysis. The Kaplan-Meier Plotter (http://kmplot.com/) (33) was used to analyze the correlation between gene expression levels and overall survival (OS), Recurrence-Free Survival (RFS) and Post-progression Survival (PPS) in colorectal cancer cohorts.

Gene set enrichment analysis. Gene Ontology (GO) and Kyoto Encyclopedia of Genes and Genomes (KEGG) enrichment analyses were performed on the related genes and co-expressed genes using the clusterProfiler package (version 4.4.4; https://CRAN.R-project.org/package=clusterProfiler) to identify overrepresented biological processes and pathways.

Immune infiltration analysis. For the immune infiltration analysis, the single-sample gene set enrichment analysis (ssGSEA) algorithm provided in the R package GSVA (version 1.46.0; https://bioconductor.org/packages/release/bioc/html/GSVA.html) was used to calculate the correlation between CXCL9 and immune cells. The Tumor Immune System Interaction Database (TISIDB) (http://cis.hku.hk/TISIDB/) was employed to analyze the chemokines and chemokine receptors related to CXCL9. TISIDB is a comprehensive database that integrates multi-omics data related to the interaction between tumors and the immune system. It contains information from various sources, including genomics, transcriptomics, proteomics and immunology. This database enables researchers to explore the complex relationships between tumor-associated genes, immune cell infiltration, immune-related pathways, and therapeutic responses (34).

Prediction of m6A sites. Target RNA sequences were obtained from the National Center for Biotechnology Information (NCBI; https://www.ncbi.nlm.nih.gov). The NCBI is a leading bioinformatics hub under the U.S. National Library of Medicine, offering extensive biological databases, such as GenBank, and powerful analysis tools, such as BLAST, to support global scientific research in genetics, genomics and molecular biology. The prediction of m6A methylation sites was performed using the sequence-based RNA adenosine

methylation site predictor (SRAMP; http://www.cuilab.cn/sramp) database. SRAMP is a mammalian m6A sites predictor, which was constructed by extracting and integrating sequence and predicted structural features around m6A sites within a machine learning framework. It shows promising performance in cross-validation tests on its training dataset and in rigorous independent tests (35).

Cell culture. The human colorectal cancer cell line SW480, RKO and the human kidney epithelial cell line 293T were procured from the American Type Culture Collection. Cells were routinely cultured in Dulbecco's Modified Eagle's Medium (DMEM; Gibco; Thermo Fisher Scientific, Inc.) supplemented with 10% fetal bovine serum (FBS; Zhejiang Tianhang Biotechnology Co., Ltd.), 1% penicillin-streptomycin solution. Cells were maintained at 37˚C in a humidified incubator with 5% CO_2.

Design and validation of siRNA. To initiate the present study, three distinct small interfering (si)RNA oligonucleotides were designed specifically targeting the coding sequence of ALKBH5, as well as a scrambled negative control sequence (Table SI). These siRNA sequences were synthesized by Beijing Tsingke Biotech Co., Ltd. Subsequently, each siRNA (at a concentration of 50 nM) was transiently transfected into RKO cells cultured in 6-well plates using Lipofectamine 2000® (Invitrogen; Thermo Fisher Scientific, Inc.; cat. no. 11668019) at 37˚C for 24 h. This process was conducted to evaluate the knockdown efficiency of each siRNA (Fig. S1A). Based on the results, the siRNA sequence with the highest knockdown efficiency (GAAAGGCTGTTGGCATCAATA) was selected to design shRNA primers for further construction of the knockdown vector.

Construction of vectors. For the overexpression vector, the pCDH plasmid was used as the backbone. For the knockdown vector, the pLKO.1 plasmid was employed. The primers used for amplification and annealing were designed based on the sequences provided in Table SI. These primers, along with the empty vectors, were synthesized or purchased by Beijing Tsingke Biotech Co., Ltd. The detailed procedure involved PCR amplification of the target sequences or annealing of primers at high temperatures, followed by restriction enzyme digestion of the vectors. For the overexpression vector, the pCDH vector was digested using EcoRI (NEB, R3101VVIAL) and BamHI (NEB, R3136VVIAL) restriction enzymes, For the knockdown vector, the pLKO.1 vector was digested using AgeI (NEB, R3552SVIAL) and EcoRI (NEB, R3101VVIAL) restriction enzymes. Homologous recombination (2X MultiF Seamless Assembly Mix, ABclonal, cat. no. RM20523) was performed to integrate the target sequences into the vectors. The ligation products were transformed into competent DH5α cells, which were subsequently cultured overnight at 37˚C. Single colonies were selected and further verified by sequencing to ensure the successful construction of the vectors.

Lentivirus packaging and infection. To achieve efficient gene knockdown and overexpression, a lentivirus vector system was employed. For lentivirus packaging, 293T cells were co-transfected with a mixture of the recombinant vector or the control vector, the pCMV-VSV-G envelope vector, and the pCMV-Gag-Pol packaging vector (both from Promega Corporation) at a 4:3:1 ratio (totaling 10 μg of DNA) using the PEI reagent (Polyplus-transfection SA). The cells were then incubated at 37˚C for 72 h. Following incubation, the viral supernatant was collected and filtered through a 0.22-μm filter to remove cellular debris. The viral titer was determined using the Lenti-Pac™ HIV qRT-PCR Titration Kit (GeneCopoeia, Inc.). Subsequently, the lentivirus was used to infect RKO cells at a multiplicity of infection of 5. After infection, puromycin was applied to select stable RKO cell lines.

Reagents. 3-Methyladenine (3-MA, MCE) was prepared in DMSO and stored at -80˚C until use. Actinomycin D was purchased from MilliporeSigma. Stock solutions were prepared in sterile distilled water at a concentration of 1 mg/ml and stored at -20˚C until use. 3-MA was used at a final concentration of 1 mM. Actinomycin D was used at a final concentration of 5 μg/ml.

Reverse transcription-quantitative (RT-q) PCR. RNA extraction, cDNA synthesis and qPCR performed according to the manufacturer's protocols. All experiments were repeated at least three times. Total RNA was isolated from cellular samples using the Ultrapure RNA Kit, a product of CWBio. Subsequent to RNA extraction, the Reverse Hifair® III 1st Strand cDNA Synthesis SuperMix for qPCR, manufactured by Shanghai Yeasen Biotechnology Co., Ltd., was used to perform reverse transcription, converting the isolated total RNA into complementary DNA (cDNA). Following this, the 2X Universal Blue SYBR Green qPCR Master Mix (with UDG), provided by Wuhan Servicebio Technology Co., Ltd., was employed for qPCR, which was conducted on the CFX Connect Real-Time PCR Detection System (Bio-Rad Laboratories, Inc.), under the following thermal cycling conditions: Initial denaturation step at 95˚C for 10 min, followed by 40 cycles consisting of denaturation at 95˚C for 10 sec, annealing at 60˚C for 20 sec, and extension at 72˚C for 15 sec. Relative gene expression was quantified using the comparative Cq ($2^{-\Delta\Delta Cq}$) method (36), with GAPDH serving as an endogenous reference gene for normalization of the data. The primers used for qPCR were shown in Table SII.

Cell proliferation assays. The Cell Counting Kit-8 (CCK-8) assay was employed to quantitatively assess cell proliferation. Cells were seeded at a density of $1x10^4$ cells per well in 96-well plates and incubate at 37˚C with 5% CO_2 for 12 h to allow for cell adhesion. After cells attached to 96-well plate for 0-120 h, 10 μl of the Cell Counting Kit-8 (Dalian Meilun Biology Technology Co., Ltd.) was added to each well and incubated for 1 h at 37˚C. Subsequently, the optical density of the samples was measured using a spectrophotometer, with the wavelength set to 450 nm which is indicative of viable cell count.

Transwell assay. The upper aspect of the Transwell membrane was uniformly layered with Matrigel, followed by a 30-min incubation period at 37˚C to facilitate solidification. Subsequently, a cellular suspension consisting of $1x10^5$ cells in 100 μl of serum-free medium was dispensed into the upper

chamber of each Transwell insert. Concurrently, the lower chamber was supplemented with 600 μl of medium enriched with 10% serum to act as a chemotactic agent. After being incubated for 20 h at 37˚C, the cells remaining at the upper surface of the membrane were removed by a cotton swab. The cells that had successfully traversed to the inferior surface of the membrane were then immobilized using a 4% paraformaldehyde solution for a 15-min fixation at room temperature and stained with 1X modified Giemsa stain (Beyotime Institute of Biotechnology) for 45 min at room temperature. The migratory cells on the underside of the membrane were subsequently captured using a fluorescence microscope for documentation.

Cell wound healing assay. Once a confluent monolayer was established, the cell monolayers were subjected to mechanical wounding via a sterile 200 μl micropipette tip to create a standardized wound. To eliminate cellular debris and ensure accurate wound assessment, the wounded monolayers were copiously rinsed with PBS multiple times. Subsequently, the cells were maintained in a serum-free medium for a duration of 72 h to simulate wound healing conditions. The progression of *in vitro* wound closure was monitored using a fluorescent microscope at designated time intervals. The *in vitro* wound healing was recorded and assessed using the closure rate, which was calculated as follows: [(Wound area at 0 h-Wound area at x h)/Wound area at 0 h] x100%.

Western blotting. Cells were subjected to lysis in a RIPA buffer, which was complemented with Phenylmethanesulfonyl Fluoride (PMSF, Beyotime Institute of Biotechnology). The resultant lysate was centrifuged at 12,000 x g for a duration of 15 min at 4˚C to achieve clarification. Subsequently, the protein concentration within the supernatant was ascertained using a BCA (Beyotime Institute of Biotechnology; cat. no. P0012) assay. The Omni-Easy™ One-step Color PAGE Gel Rapid Preparation Kit (Epizym, Inc.; PG211 and PG213) was used to prepare 7.5 and 12.5% gels. An aliquot of the protein lysate, containing 20 μg of total protein, was resolved on SDS-PAGE and subsequently transferred onto PVDF membrane (MilliporeSigma; cat. no. IPVH00010). The membranes were pre-incubated with a blocking solution consisting of 5% non-fat milk for 1 h at room temperature. Thereafter, the membranes were incubated with the respective primary antibodies at 4˚C overnight. Following this incubation, the membranes were washed thoroughly and then exposed to anti-rabbit/mouse/rat secondary antibodies for 1 h at room temperature. The immunoreactive bands were visualized using an ECL substrate (Biosharp Life Sciences; cat. no. BL520A), and the membrane was detected using a chemiluminescence imaging system (eBlot). Primary antibodies used in this study were: Mouse anti-GAPDH (1:5,000; Proteintech Group, Inc.; cat. no. 60004-1-Ig), rabbit anti-LC3B (1:1,000; ABclonal Biotech Co., Ltd.; cat. no. A11282), rabbit anti-P62 (1:2,000; ABclonal Biotech Co., Ltd.; cat. no. A19700), rabbit anti-CXCL9/MIG (1:1,000; ABclonal Biotech Co., Ltd.; cat. no. A25183); and the secondary antibodies were: HRP Goat Anti-Rat IgG (H+L; 1:10,000; ABclonal Biotech Co., Ltd.; cat. no. AS028), HRP Goat Anti-Mouse IgG (H+L; 1:10,000; ABclonal Biotech Co., Ltd.; cat. no. AS003) and HRP Goat Anti-Rabbit IgG (H+L; 1:10,000; ABclonal Biotech Co., Ltd.; cat. no. AS014). The gray value was measured by ImageJ software (version 1.54f; National Institutes of Health).

Methylated RNA immunoprecipitation sequencing (MeRIP-seq). Total RNA was extracted from cells, for both the IgG group and the m6A group, 100 μg of total RNA was added, along with an appropriate quantity of RNase inhibitor. Subsequently, 1 μl of either IgG antibody (Proteintech Group, Inc.; cat. no. B900620; for the IgG group) or m6A antibody (Proteintech Group, Inc.; cat. no. 68055-1-Ig; for the m6A group) was introduced. IP buffer was then supplemented to adjust the volume to 200 μl. After thorough mixing, the samples in both groups were incubated overnight at 4˚C. Protein A/G Magnetic beads are washed with IP buffer, and the premix is added and incubated at 4˚C for 3 h. The beads with bound RNA are washed 4-5 times with IP buffer. After adding TRIzol® (Thermo Fisher Scientific, Inc.) an RNA purification kit (CWBio.) to was used to extract the RNA on the magnetic beads. The purified m6A-enriched RNA were analyzed by RT-qPCR as aforementioned to quantify specific m6A/modified RNAs.

Statistical analysis. All data analyses were conducted using GraphPad Prism software, version 8.0.1 (Dotmatics). The experimental groups were compared using the non-parametric two-tailed Student's t-test to assess the statistical significance between two independent samples. For multiple group comparisons, a one-way analysis of variance was employed, followed by Tukey's post hoc test to correct for multiple comparisons and to identify the source of significant variance within the dataset. Each treatment condition for the cellular samples was replicated a minimum of three times to ensure the reproducibility and reliability of the experimental outcomes. Data are presented as the mean ± standard error of the mean to reflect the variability within the sample set. P-values are reported for all statistical tests. $P<0.05$ was considered to indicate a statistically significant difference. Specific P-values are indicated in the figure legends and results sections ($^{*}P<0.05$, $^{**}P<0.01$, $^{***}P<0.001$).

Results

Expression patterns and prognostic models of CXCL family in COAD. Variance analysis indicated that the CXCL family displayed significant differential expression in COAD, as presented in Fig. 1A. A prognostic model of CXCL family in COAD was constructed through LASSO regression, which has good diagnostic value (Fig. 1B-E). COX regression analysis was performed on seven genes in the prognostic model of CXCL family (Fig. 1F), and the association between molecular and methylation genes with $P<0.2$ in univariate regression was analyzed. The results showed that CXCL8, CXCL9, and CXCL11 have an association with methylation genes (Fig. 1G). The PPI network with CXCL family and their interacting genes shows that CXCL9 is the hub gene with the highest degree score in the prognostic model genes of the CXCL family (Fig. 1H).

Expression of CXCL9 in pan-cancer and COAD. Considering the significant role of CXCL9 in the prognostic model of the

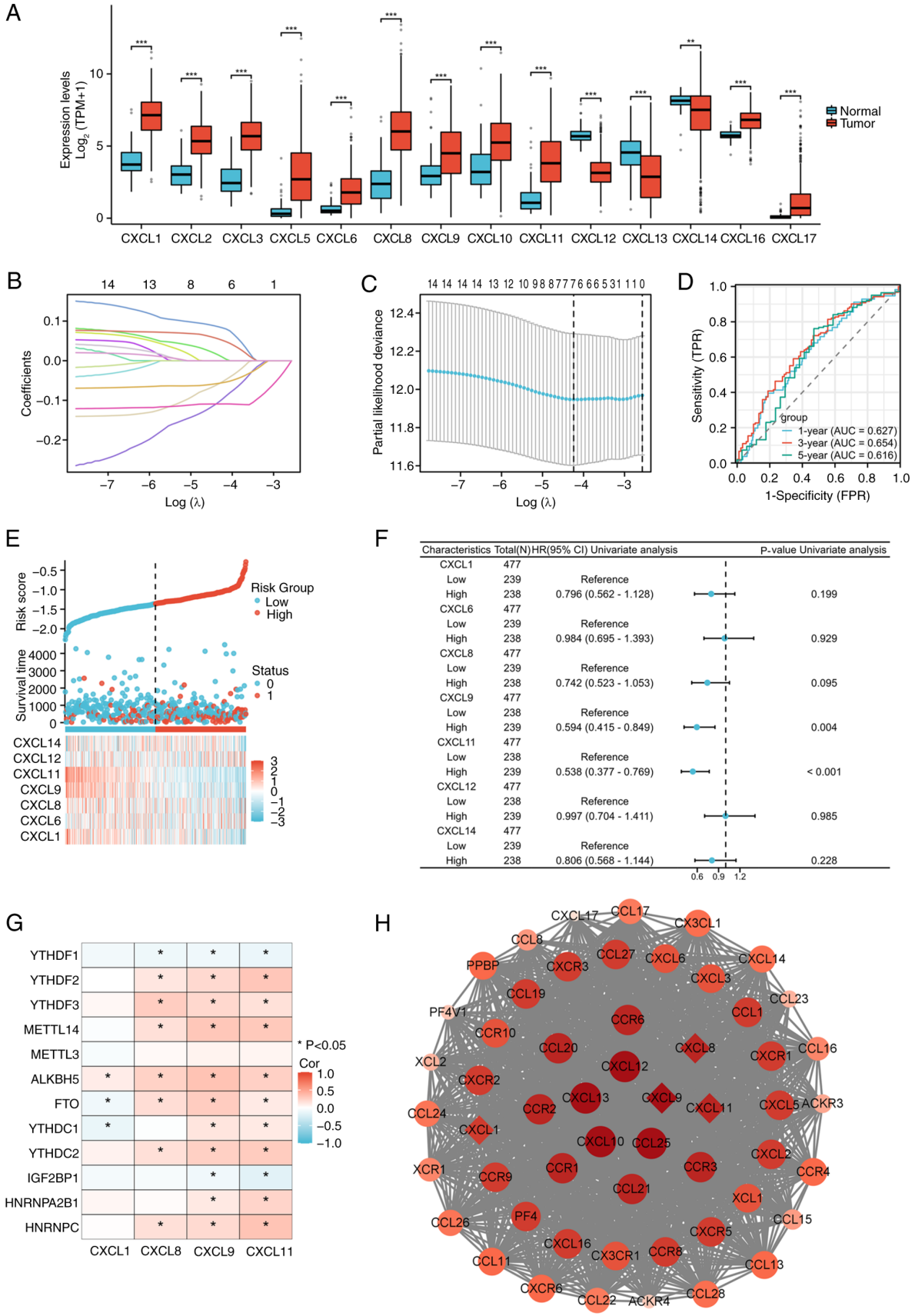

Figure 1. Construction of a prognostic CXCL family model for COAD. (A) Expression patterns of the CXCL family in COAD. (B) Lasso coefficient spectrum of CXCL family genes. (C) Cross-validation for selection of the tuning parameter in a proportional hazards model. (D) ROC curves for the CXCL family risk model in the TCGA-COAD cohort. (E) Distribution of risk scores, survival status, and expression profiles of CXCL model genes in the TCGA-COAD dataset (Sample size: 521). (F) Prognostic forest plot of CXCL family risk model genes. (G) Relationship between prognostic CXCL family genes and m6a-related genes. (H) PPI network diagram of CXCL family and interacting genes, the top ten genes with the highest degree scores were displayed in red and genes in CXCL family risk model were marked with diamonds. *P<0.05, **P<0.01, ***P<0.001. CXCL, C-X-C motif chemokine ligand; COAD, colorectal adenocarcinoma; ROC, receiver operating characteristic; TCGA, The Cancer Genome Atlas; PPI, protein-protein interaction; AUC, area under the curve; Cor, correlation.

CXCL family, the expression of CXCL9 in cancer was further analyzed, particularly in COAD, as well as its effect on the prognosis of COAD patients. Results showed that CXCL9 is highly expressed in most types of cancer (Fig. 2A) and is markedly associated with patient PFI in cancers such as breast cancer (BRCA), COAD, KIRP, LGG, SARC and UCEC (Fig. 2B). The TCGA and GSE41258 dataset from GEO indicated that CXCL9 was highly expressed in COAD (Fig. 2C and D). An analysis of the relationship between CXCL9 expression and various clinical indicators in the TCGA dataset revealed that CXCL9 expression exhibited a trend of first increasing and then decreasing with the progression of COAD (Fig. 2E). Slight differences in CXCL9 expression were observed among different ethnicities and in different residual tumor classifications (Fig. 2F and G). KMplot showed that patients with elevated CXCL9 expression exhibited markedly improved OS, RFS and PPS compared to those with lower expression levels (Fig. 2H-J).

Molecular mechanisms and pathway enrichment of CXCL9. To further clarify the molecular mechanisms underlying the role of CXCL9 in COAD, the present study conducted enrichment analyses using the GO, KEGG and GSEA. GO and KEGG enrichment analysis was performed using the top 200 most-associated genes. The EMAP plot revealed significant enrichment of CXCL9 and its associated genes in pathways related to T cell activation and leukocyte adhesion (Fig. 3A). In GSEA enrichment analysis using co-expressed genes, numerous pathways related to the functions of T cells and B cells were identified, such as Co-stimulation by the CD28 family and CD22 mediated BCR regulation (Fig. 3B). In addition, pathways related to Fc epsilon Receptor I (FcεRI) and mitochondria related pathways as well as DNA methylation, and the Wnt Beta catenin signaling pathway, cell surface interactions at the vascular wall and others were also enriched (Fig. 3C-H). GO and KEGG combined with FC bubble chart demonstrated a correlation with the cell cycle related pathway (Fig. 3I).

CXCL9 is associated with immune infiltration and exhibits differential immune infiltration patterns across various stages. Immune infiltration analysis indicated that CXCL9 in CRC was positively associated with the majority of immune infiltration cells, predominantly cytotoxic cells, activated dendritic cells (aDC), Th1 cells, and T cells (Fig. 4A). The effect of CXCL9 on CRC immune infiltration varies across different stages of cancer progression. In Stage I, CXCL9 shows a positive correlation with cytotoxic cells, aDC, and Th1 cells (Fig. 4B). In Stage III, it maintains a positive correlation with cytotoxic cells, macrophages, and T cells (Fig. 4D). In Stage IV, the positive correlation was observed with cytotoxic cells, Th1 cells and CD8 T cells (Fig. 4E). However, a notable alteration in immune infiltration is observed in Stage II, where CXCL9 exhibited a negative correlation with numerous immune cells, including cytotoxic cells, aDC, macrophages, Th1 cells, T cells, and neutrophils (Fig. 4C). The TISIDB analysis suggested that CXCL9 in COAD was most closely associated with chemokines CCL4, CCL5, CCL8, CCL18, CXCL10, CXCL11 and CXCL13, as well as chemokine receptors CCR1, CCR2, CCR5, CCR8 and CXCR6 (Fig. S2A and B). Therefore, the expression of these chemokine receptors in different stages of COAD was analyzed and it was found that the expression patterns of CCR5, CCR8 and CXCR6 were similar to CXCL9 (Fig. S2C).

CXCL9 is highly expressed in colorectal cancer and markedly enhances the malignant traits of colorectal cancer cells. Subsequent to bioinformatics analysis of CXCL9, *in vitro* assays were performed to explore its potential role in promoting tumor growth in colorectal cancer cells. In colon cancer cell lines, the expression of the CXCL9 gene was examined and it was found that its expression level was markedly higher in RKO and SW480 cells compared to NCM460 (Fig. 5A). Through qPCR and western blotting validation, cell lines with overexpression of CXCL9 were successfully constructed (Fig. 5B-D).

Wound healing assays were performed to assess the effect of CXCL9 overexpression on cell migratory capacity. The results demonstrated that cells overexpressing CXCL9 closed the wound area more rapidly than control cells within 48 h (Fig. 5E and F). The invasive potential of colorectal cancer cells with CXCL9 overexpression was further evaluated through Transwell assays. Notably, the number of cells that traversed the chamber was markedly higher when compared with the control cohort (Fig. 5G and H), indicating a significant increase in invasiveness ($P<0.01$) attributed to the overexpression of CXCL9. CCK-8 assays were utilized to measure the impact of CXCL9 overexpression on cell proliferation. The absorbance at OD450, which reflects cell viability, showed that cells with overexpressed CXCL9 exhibited a higher proliferation rate during 0-120 h (Fig. 5I). These results indicated a potential role of CXCL9 in the progression of colorectal cancer.

Overexpression of CXCL9 can regulate autophagy. The present study treated SW480 and RKO cells with 3-MA and found changes in the expression of the CXCL9 gene within 0-8 h (Fig. 6A and B). These observations suggested a potential role of CXCL9 in autophagy regulation Following CXCL9 overexpression, an increase in the RNA levels of autophagy-related genes was observed, indicating a potential involvement of CXCL9 in the regulation of autophagic flux (Fig. 6C). Western blotting results indicated that overexpression of CXCL9 can inhibit the degradation of p62 and suppress the conversion of LC3-I to LC3-II, thereby blocking autophagy flux (Fig. 6D).

Regulation of CXCL9 by the m6A Eraser ALKBH5 in CRC. SRAMP identified a high-confidence m6A methylation site within the CXCL9 gene (Fig. 7A and B). This implied that CXCL9 may be subject to post-transcriptional regulation through m6A modification, which could have significant implications for its expression and function in cellular processes. Through bioinformatics analysis, a strong correlation between CXCL9 and the m6A eraser ALKBH5 was predicted (Fig. 7C). Consequently, the expression levels of CXCL9 in cell lines with ALKBH5 knockdown and overexpression were examined. The results showed that the expression of CXCL9 increased in response to ALKBH5 overexpression and decreased following ALKBH5 knockdown (Fig. 7D and E). Actinomycin D chase experiments revealed that the stability of CXCL9 was markedly reduced in ALKBH5 knockdown cells compared to the control group,

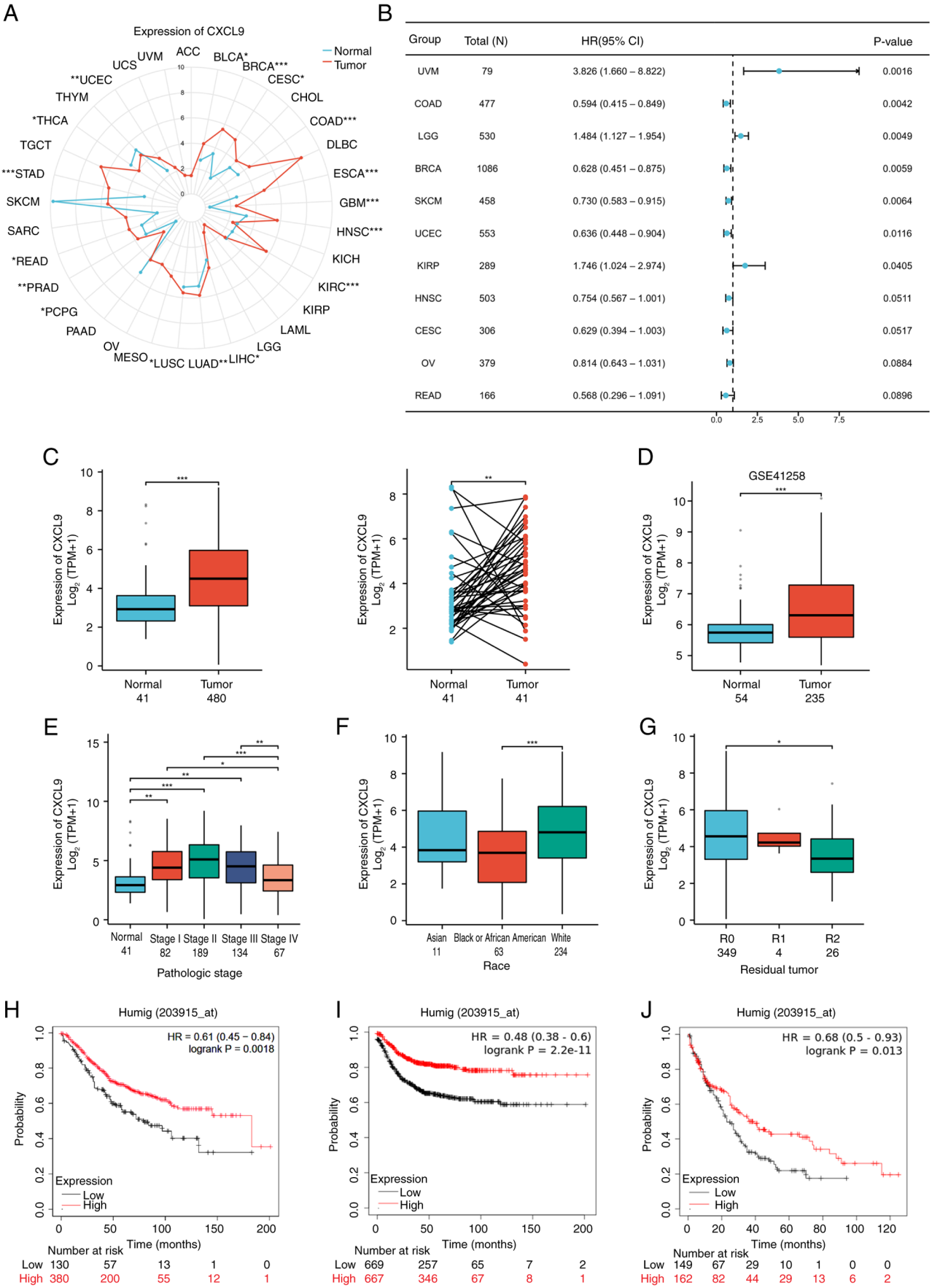

Figure 2. CXCL9 expression in pan-cancer and BRCA. (A) CXCL9 expression in pan-cancer based on TCGA database. (B) The prognostic forest plot of CXCL9 in pan-cancer. (C and D) CXCL9 expression in COAD based on TCGA database and the GEO database. Relationship between CXCL9 expression and clinicopathological characteristics of patients with COAD: (E) Pathologic stage; (F) ethnicity; (G) Residual tumor. (H-J) The Kaplan-Meier plot of CXCL9 in COAD. *P<0.05, **P<0.01, ***P<0.001. CXCL, C-X-C motif chemokine ligand; BRCA, breast cancer; TCGA, The Cancer Genome Atlas; COAD, colorectal adenocarcinoma; HR, hazard ratio.

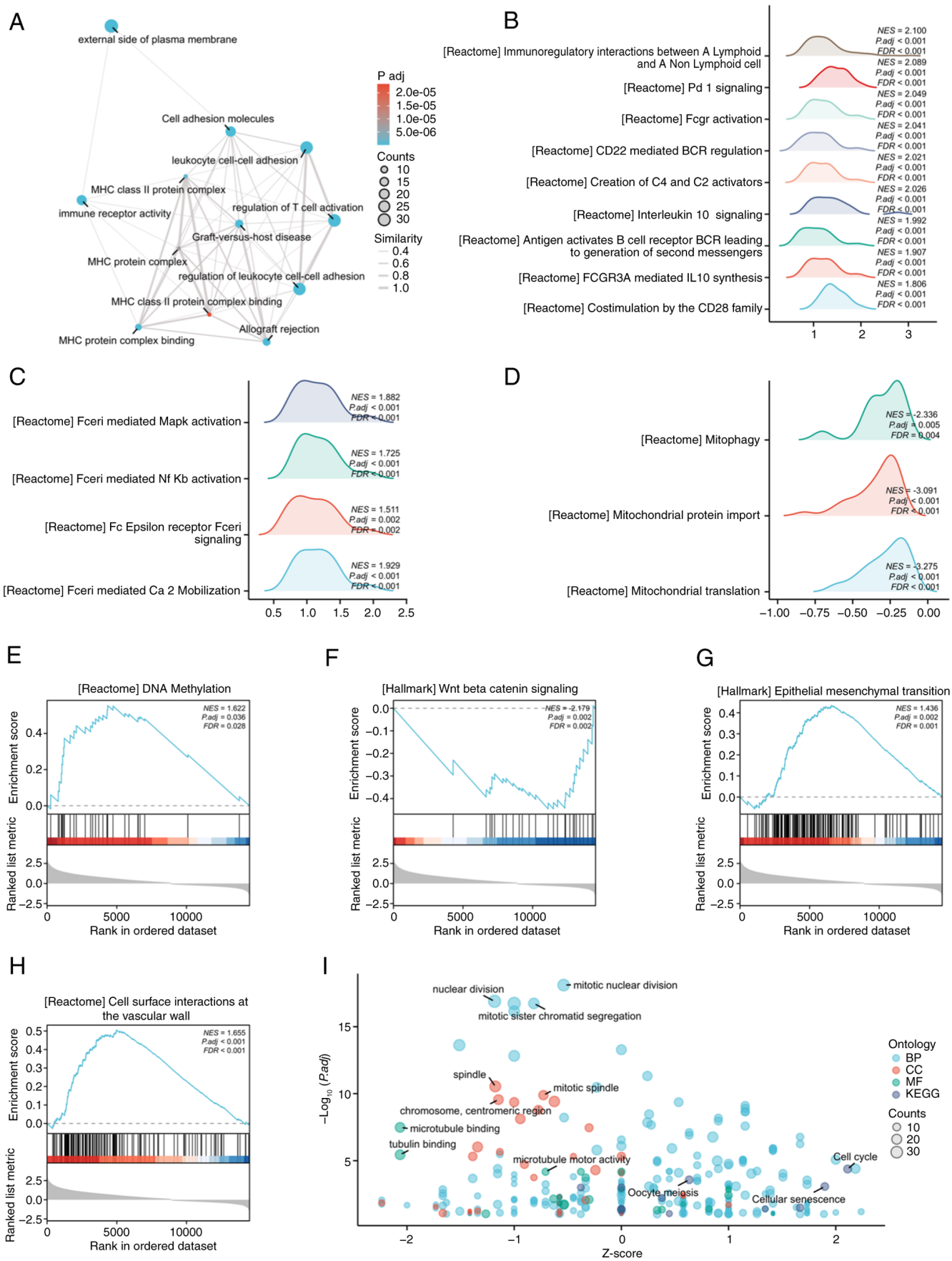

Figure 3. Functional Clustering Analysis of CXCL9-Associated Genes and Co-expressed Genes. (A) Enrichment Map of GO/KEGG enrichment. (B-D) GSEA Enrichment Analysis Plots: (B) Immune-related pathways, (C) FCERI pathway, (D) Mitochondrial function-related pathways. (E) DNA Methylation. (F) Wnt β-catenin signaling. (G) Epithelial-mesenchymal transition. (H) Cell surface interactions at the vascular wall. (I) Bubble plot of GO/KEGG combined logFC. CXCL, C-X-C motif chemokine ligand; GO, Gene Ontology; KEGG, Kyoto Encyclopedia of Genes and Genomes; GSEA, gene set enrichment analysis; FcεRI,, Fc epsilon Receptor I; BP biological process; CC cellular component; MF molecular function.

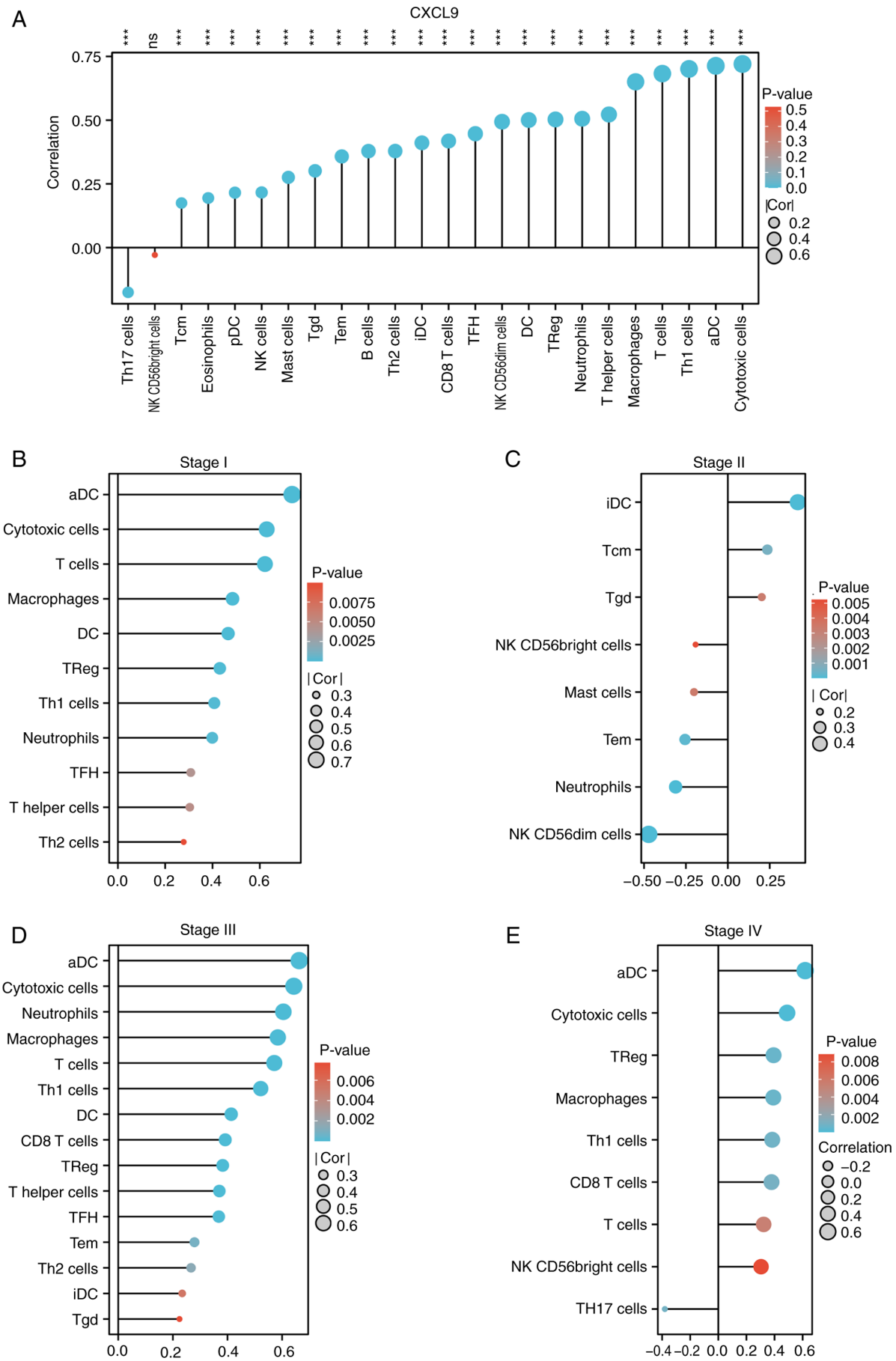

Figure 4. Analysis of CXCL9 expression and immune cell infiltration across different stages of COAD. Correlation analysis between CXCL9 expression levels and various immune cell types across different stages of COAD. (A) All stages; (B) Stage I; (C) Stage II; (D) Stage III; (E) Stage IV. ***P<0.001. CXCL, C-X-C motif chemokine ligand; COAD, colorectal adenocarcinoma; Cor, correlation.

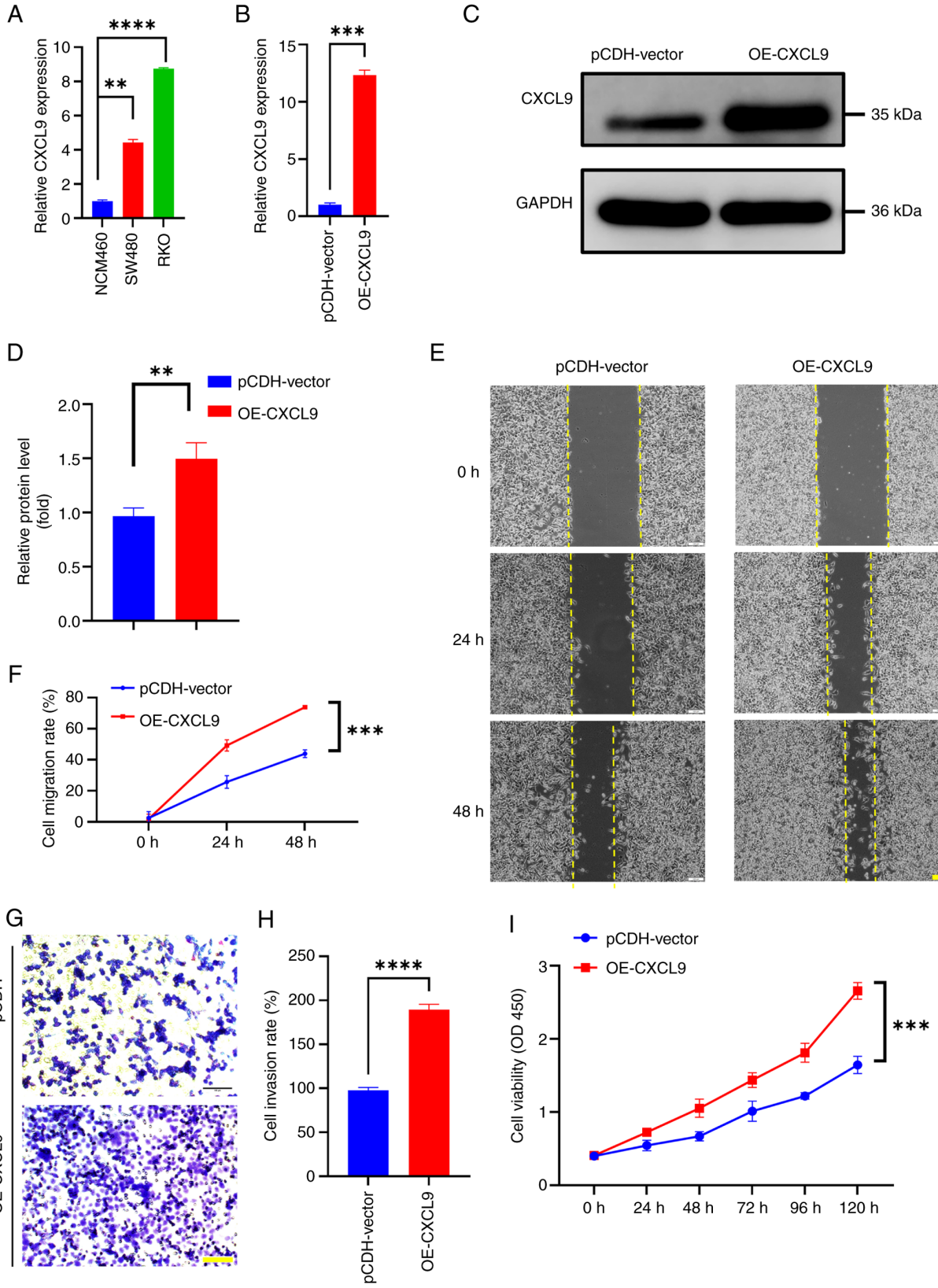

Figure 5. CXCL9 is related to colorectal cancer cell proliferation, migration and invasion. (A) Expression of CXCL9 in colon cancer cell lines (t-test of SW480 vs. NCM460: P=0.0013, 95% confidence interval: 2.904-3.964, η^2=0.9974; t-test of RKO vs. NCM460: P<0.0001, 95% confidence interval: 7.465-7.998, η^2=0.9999). (B-D) Validation of stable cell construction by quantitative PCR (t-test of OE-CXCL9 vs. pCDH-vector: P=0.0008, 95% confidence interval: 9.961 to 12.71, η^2=0.9984) and western blotting (OE-CXCL9 vs. pCDH-vector: P=0.0054, 95% confidence interval: 0.2612 to 0.7961, η^2=0.8828). (E and F) The effect of overexpressing CXCL9 on the migration ability of colon cancer cells (scale bar, 100 μm; mutiple t-test of OE-CXCL9 vs. pCDH-vector: 24 h P<0.001, difference=23.5070; 48 h P<0.001 difference=29.9395). (G and H) The effect of overexpressing CXCL9 on the invasion ability of colon cancer cells (scale bar, 100 μm; t-test of OE-CXCL9 vs. pCDH-vector: P<0.0001, 95% confidence interval: 80.87 to 102.6, η^2=0.9928]. (I) The effect of overexpressing CXCL9 on the proliferation ability of colon cancer cells. Data are expressed as means ± SEM from at least three experiments (multiple t-test of OE-CXCL9 vs. pCDH-vector: 24 h P=0.006, Difference=0.18; 48 h P=0.001, Difference=0.3825; 72 h P=0.002, Difference=0.425; 96 h P<001, Difference=0.59; 120 h P<001, Difference=1.0125). **P<0.01, ***P<0.001, ****P<0.0001. CXCL, C-X-C motif chemokine ligand; OE, overexpression.

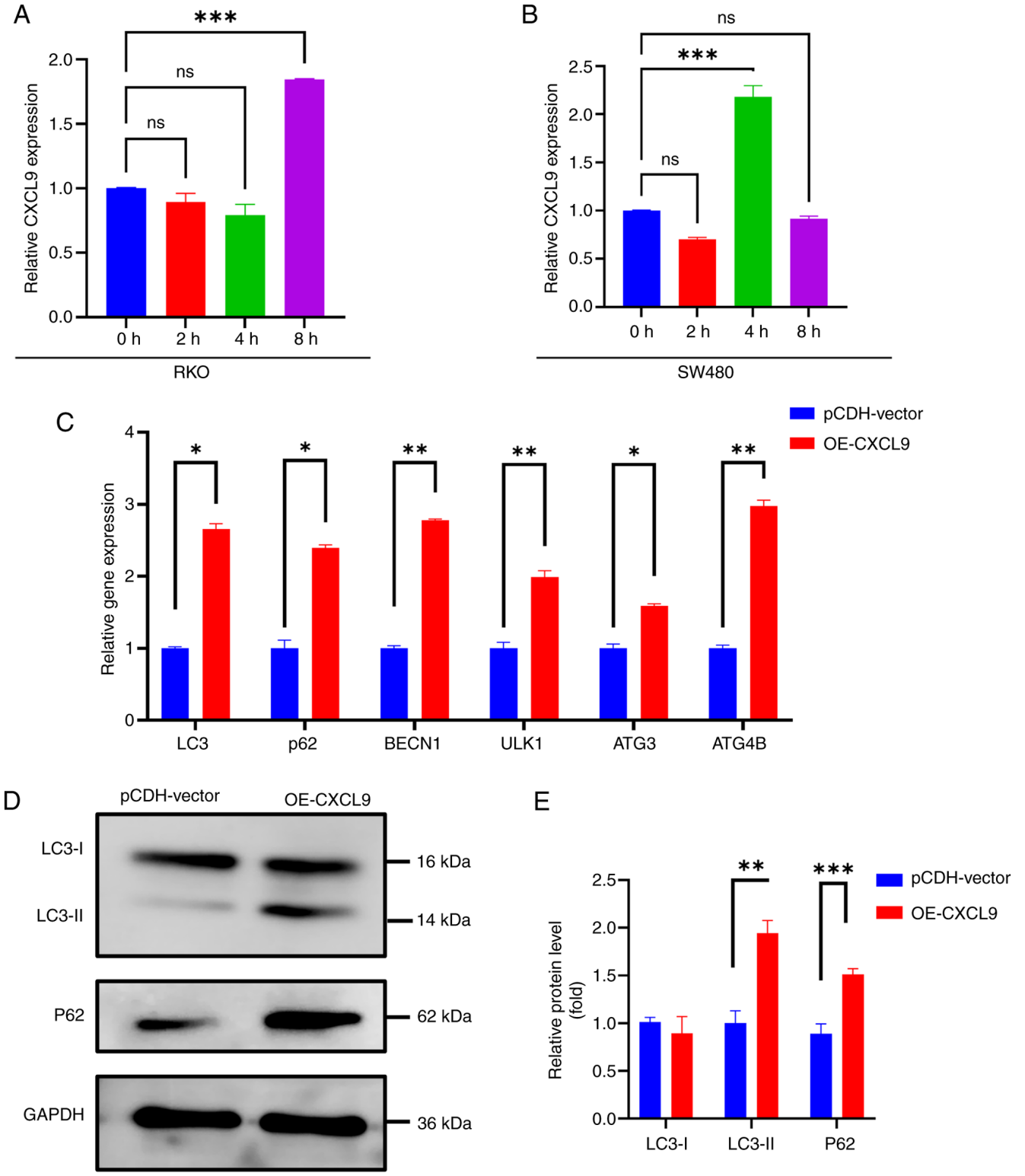

Figure 6. CXCL9 is associated with autophagy. Changes in the CXCL9 gene in colon cancer cells after the addition of 3-MA: (A) RKO (One-way ANOVA of 8 h vs. 0 h: P=0.0009, 95% confidence interval: 1.120-0.5686, η^2=0.9836). (B) SW480 (One-way ANOVA of 4 h vs. 0 h: P=0.0004, 95% confidence interval: 1.491-0.8686, η^2=0.9890). (C) The effect of CXCL9 gene overexpression on the mRNA expression of autophagy-related genes (multiple t-test of OE-CXCL9 vs. pCDH-vector: LC3 P=0.001, Difference=1.65802; p62 P=0.004, Difference=1.38966; BECN1 P<0.001, Difference=1.78132; ULK1 P=0.008, Difference=0.98638; ATG3 P=0.006, Difference=0.591265; ATG4B P=0.001, Difference=1.97811). (D and E) The influence of CXCL9 gene overexpression on the protein expression levels of LC3 and P62 (multiple t-test of OE-CXCL9 vs. pCDH-vector: LC3-II P<0.001, Difference=0.942989; P62 P<001, Difference=0.623079). *P<0.05, **P<0.01, ***P<0.001. ns; no significance. CXCL, C-X-C motif chemokine ligand; OE, overexpression.

while overexpression of ALKBH5 markedly enhanced the stability of CXCL9 (Fig. 7F and G). The MeRIP experiment demonstrated that the m6A level of CXCL9 decreased upon overexpression of ALKBH5, while it increased upon the knockdown of ALKBH5 (Fig. 7H and I). The present study stably expressed a knockdown of ALKBH5 in RKO cells and

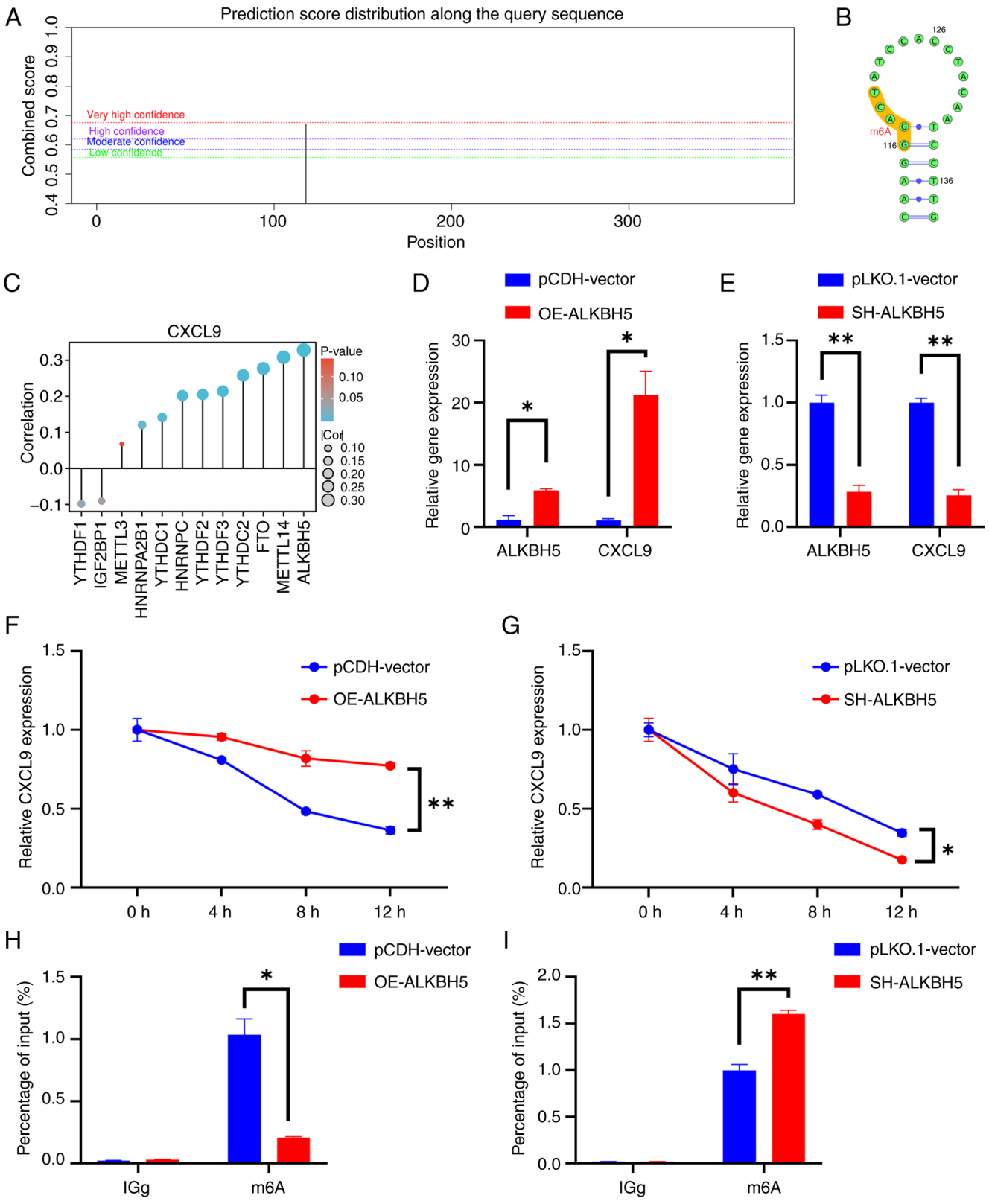

Figure 7. ALKBH5 mediates the demethylation modification of CXCL9 to enhance its stability. (A) SRAMP-predicted m6A modification sites of CXCL9 and (B) the secondary structure of RNA. (C) Correlation between CXCL9 and m6A-related gene expression. (D and E) The effect of overexpression and knockdown of the m6A eraser ALKBH5 on CXCL9 mRNA expression (t-test of OE-ALKBH5 vs. pCDH-vector, ALKBH5: P=0.0126, 95% confidence interval: 2.425-7.054, η^2=0.9749; CXCL9: P=0.0176, 95% confidence interval: 8.512-31.87, η^2=0.9651. t-test of SH-ALKBH5 vs. pLKO.1-vector: ALKBH5: P=0.0061, 95% confidence interval: -0.9606 to -0.4765, η^2=0.9879; CXCL9: P=0.0029, 95% confidence interval: -0.9205 to -0.5724, η^2=0.9942]. (F and G) The impact of overexpression and knockdown of the m6A eraser ALKBH5 on the stability of CXCL9 mRNA (multiple t-tests of OE-ALKBH5 vs. pCDH-vector: 4 h P=0.011, Difference=0.145836; 8 h P=0.011, Difference=0.334887; 12 h P=0.002, Difference=0.41087; multiple t-tests of SH-ALKBH5 vs. pLKO.1-vector: 8 h P=0.016, Difference=-0.190368; 12 h P=0.009, Difference=-0.170625). (H and I) Effect of ALKBH5 overexpression/knockdown on m6a level of CXCL9 (Multiple t-test of OE-ALKBH5 vs. pCDH-vector, m6A: P=0.012, Difference=-0.826860; multiple t-test of SH-ALKBH5 vs. pLKO.1-vector, m6A: P=0.008, Difference=0.604586). *P<0.05, **P<0.01. CXCL, C-X-C motif chemokine ligand; SRAMP, sequence-based RNA adenosine methylation site predictor; OE, overexpression; SH, short hairpin RNA.

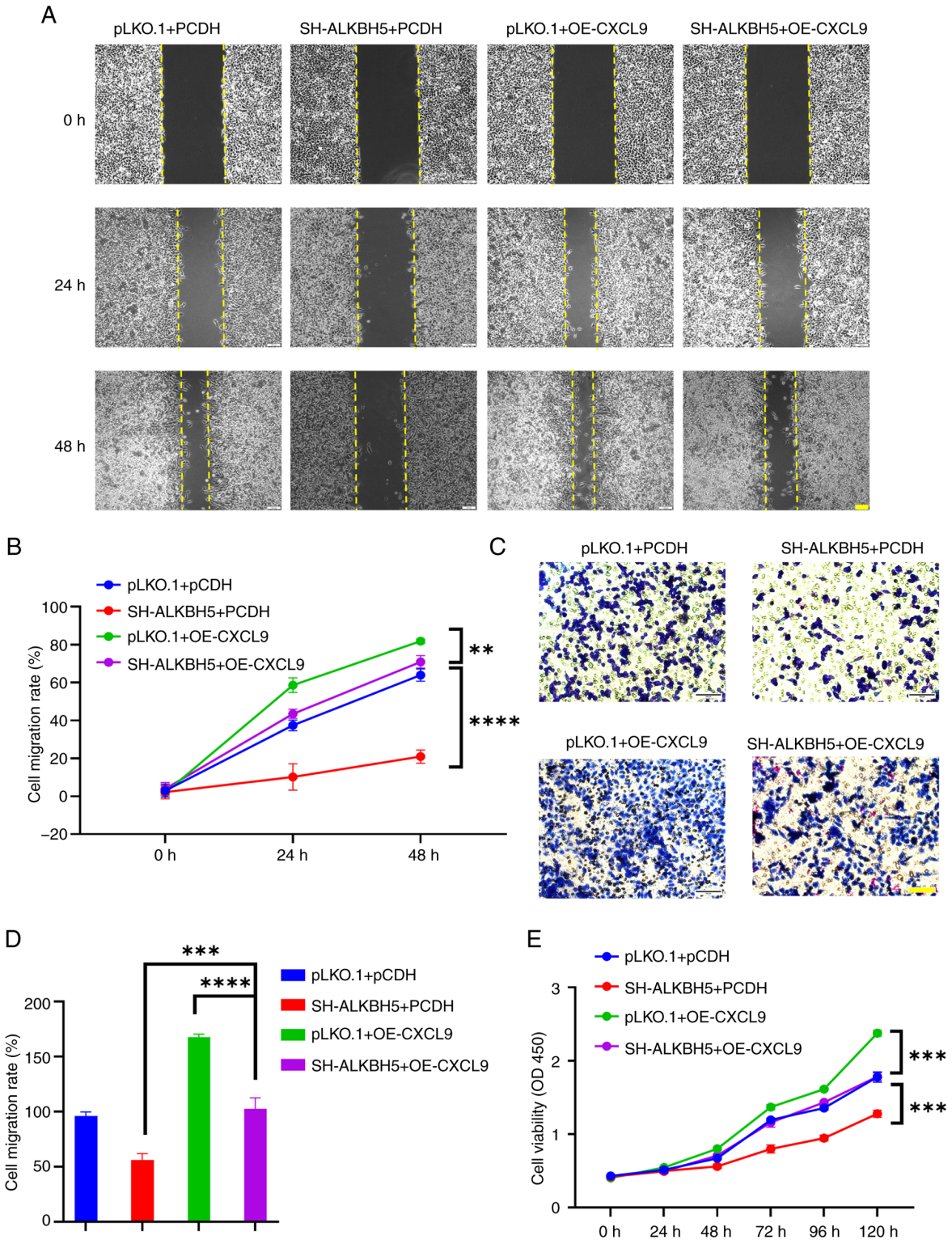

Figure 8. Overexpression of CXCL9 can counteract the effects of ALKBH5 knockdown on the development and progression of colon cancer. (A and B) The scratch assay demonstrated that overexpression of CXCL9 reversed the migration inhibition caused by ALKBH5 knockdown in RKO cells (scale bar, 100 μm; two-way ANOVA of SH-ALKBH5+PCDH vs. SH-ALKBH5 + OE-CXCL9: 24 h P<0.0001, 95% confidence interval: -41.23 to -25.34; 48 h P<0.0001, 95% confidence interval: -57.96 to -42.06. of pLKO.1+OE-CXCL9 vs. two-way ANOVA of SH-ALKBH5 + OE-CXCL9: 24 h P=0.0001, 95% confidence interval: 7.226 to 23.12; 48 h P=0.0047, 95% confidence interval: 2.949 to 18.85). (C and D) Transwell assay showed that overexpression of CXCL9 reversed the invasion inhibition caused by ALKBH5 knockdown in RKO cells (scale bar, 100 μm; one-way ANOVA of SH-ALKBH5+PCDH vs. SH-ALKBH5 + OE-CXCL9: P<0.0001, 95% confidence interval: -62.67 to -30.03; one-way ANOVA of pLKO.1+OE-CXCL9 vs. SH-ALKBH5 + OE-CXCL9: P<0.0001, 95% confidence interval: 48.87-81.50). (E) CCK-8 assay indicated that overexpression of CXCL9 reversed the proliferation inhibition caused by ALKBH5 knockdown in RKO cells (two-way ANOVA of SH-ALKBH5 + PCDH vs. SH-ALKBH5 + OE-CXCL9 48 h P<0.0001, 95% confidence interval: -0.2106 to -0.08369; 72 h P<0.0001, 95% confidence interval: -0.4235 to -0.2966; 96 h P<0.0001, 95% confidence interval: -0.5499 to -0.4230; 120 h P<0.0001, 95% confidence interval: -0.5683 to -0.4414. Two-way ANOVA of pLKO.1 + OE-CXCL9 vs. SH-ALKBH5 + OE-CXCL9: 0 h P=0.8309, 95% confidence interval: -0.08391 to 0.04296; 24 h P=0.165, 95% confidence interval: -0.01294 to 0.1139; 48 h P=0.0016, 95% confidence interval: 0.02859 to 0.1555; 72 h P<0.0001, 95% confidence interval: 0.1452 to 0.2721; 96 h P<0.0001, 95% confidence interval: 0.1173 to 0.2442; 120 h P<0.0001, 95% confidence interval: 0.5292 to 0.6560). **P<0.01, ***P<0.001, ****P<0.0001. CXCL, C-X-C motif chemokine ligand; OE, overexpression; SH, short hairpin RNA.

transiently transfected them with the OE-CXCL9 plasmid. The results from wound healing, CCK8, and Transwell assays demonstrated that CXCL9 can partially restore the effects of ALKBH5 knockdown on colorectal cancer cells (Fig. 8).

Discussion

As a subfamily of chemokines, the CXCL family not only regulates the migration of leukocytes but also controls the growth and development of tumors (17). Luo *et al* (37) demonstrated that the high-level expression of the CXCL family can result in lymph node metastasis and a higher tumor-node-metastasis stage in patients with CRC. According to numerous studies, CXCL family members have been shown to be involved in the occurrence and development of CRC closely related to its role including regulation of immune cell infiltration, tumor cell proliferation, invasion, metastasis and angiogenesis (38-40). Given the significant effect of the CXCL family on the progression of colorectal cancer, a prognostic model integrating CXCL-associated biomarkers was established utilizing data from TCGA. A comprehensive PPI network analysis of CXCL family and their interacted genes identified CXCL9 as a central node, which has a strong correlation with m6a methylation underscoring its potential as a key regulatory gene in the progression of COAD.

Bioinformatics analysis revealed significant upregulation of CXCL9 in colorectal cancer, while survival analysis demonstrated higher OS, RFS and PPS rates in patients with high CXCL9 expression. the present study conducted an analysis of CXCL9 expression at different pathologic stages and the results showed a trend of initial increase followed by decrease during cancer progression. Furthermore, within the residual tumor classification, the expression level of CXCL9 was highest in R0. The tumor microenvironment characteristics of residual tumors differ, potentially caused by CXCL9 expression and function. Low CXCL9 expression in R2 tumors may correlate with facilitating immune evasion. Given the lower baseline expression of CXCL9 in Black or African American individuals, treatment strategies are adjusted based on ethnic-specific biomarkers such as CXCL9 expression levels may be important.

The present study further investigated the mechanism of action of CXCL9 in COAD. The result of GO, KEGG and GSEA enrichment analysis demonstrated that co-expressed genes and related genes of CXCL9 were markedly enriched not only in pathways associated with immune response but also in other pathways closely related to tumorigenesis and development. Therefore, it was hypothesized that CXCL9 not only altered immune infiltration in colorectal cancer by recruiting immune cells but also influenced the initiation and progression of colorectal cancer itself.

The present study revealed a significant correlation between CXCL9 and other chemokines within the same CXC family, specifically CXCL10, CXCL11 and CXCL13. These chemokines are characterized by their ability to attract immune cells, such as T cells, natural killer (NK) cells, and monocytes, to sites of inflammation or infection (41-44). In the context of cancer, these chemokines are implicated in the recruitment of immune cells to the tumor microenvironment, where they can either promote or inhibit tumor growth depending on the context (44-47). This high correlation indicated that CXCL9 may play an important dual role in regulating tumor environment and tumor occurrence and development.

The effect of CXCL9 on immune cell infiltration in COAD varies across different stages of cancer progression. During the majority of stages, CXCL9 positively influences the recruitment of cytotoxic cells, aDC and T cells, which are critical for mounting an effective anti-tumor immune response. However, in Stage II, where CXCL9 is highest expressed, it exhibits an inverse correlation with neutrophils and NK CD56 dim cells, suggesting a shift in its role that may contribute to an immunosuppressive environment conducive to tumor progression.

The PD-1/PD-L1 axis modulates the establishment and persistence of immune tolerance within the tumor microenvironment. The interaction between PD-1 and PD-L1 or PD-L2, plays a pivotal role in regulating T cell activity, including their activation, proliferation and the secretion of cytotoxic factors in cancer. This interaction can lead to a diminishment in effective anti-tumor immune reactions (48,49). GSEA enrichment analysis indicated a positive correlation between CXCL9 expression and the PD-1 signaling pathway. When CXCL9 levels are elevated, the PD-1 signaling pathway is activated, which may suppress T cell cytotoxic activity against cancer cells. In recent years, innovations in immune checkpoint blockade therapies targeting the PD-1/PD-L1 axis have yielded surprising therapeutic outcomes in the treatment of CRC (50-52).

The aforementioned findings indicated that the influence of CXCL9 on immune cells is stage-dependent and may facilitate immune evasion during the progression of cancer, particularly in Stage II. As a prognostic marker associated with immune infiltration, CXCL9, when combined with PD-L1 therapy, could potentially represent an effective treatment strategy for Stage II CRC. *In vitro* experiments demonstrated that CXCL9 overexpression markedly contributed to the malignant characteristics of tumor cells, including cell proliferation, migration and invasion. Due to the enrichment of CXCL9 co-expressed genes in the mitophagy, further experiments were conducted to investigate the potential involvement of CXCL9 in autophagy. Following the addition of the autophagy inhibitor 3-MA, alterations in the expression of CXCL9 gene were observed. This suggested that changes in CXCL9 expression may be part of cellular adaptation to stress, as autophagy is a stress tolerance mechanism in cancer (53). In cells overexpressing CXCL9, the mRNA and protein expression levels of autophagy-related markers was assessed. qPCR results indicated that ATG3 and ATG4B were upregulated following CXCL9 overexpression, which can promote the transition from LC3-I to LC3-II and facilitating autophagosome formation (54). However, western blotting results showed an accumulation of LC3-II and p62, which suggested autophagy flow was blocked. The experimental findings suggested that the overexpression of CXCL9 may lead to the accumulation of autophagosomes and impair their degradation.

Coupled with the results from GSEA analysis showing a negative correlation between mitophagy, mitochondrial protein import and CXCL9 expression, it was hypothesized that the overexpression of CXCL9 might disrupt mitophagy, thereby blocking autophagic flux. GSEA results indicated that CXCL9 was positively associated with the MAPK and NF-κB

pathways, while it was negatively associated with the Wnt signaling pathway. Additionally, CXCL9 showed a negative correlation with pathways associated with mitophagy. Studies have revealed that the MAPK pathway, when inhibited, can lead to the activation of mitophagy through PINK1 and OPTN-dependent mechanisms, highlighting its complex role in regulating mitochondrial autophagy (52,55,56). NF-κB signaling is a key driver of mitochondrial dysfunction and morphological changes, redox imbalance, and insulin signaling disruption (57,58). Based on the *in vitro* experiments, it was hypothesized that CXCL9 may inhibit mitophagy by activating the MAPK and NF-κB pathways, thereby affecting mitophagy from multiple angles.

The present study delved into the intricate interplay between CXCL9 and ALKBH5. Existing studies have demonstrated that ALKBH5 influences gene expression levels by affecting the stability of its mRNA (59). Through a series of experiments, it demonstrated that ALKBH5 can indeed influence the stability of CXCL9 mRNA, thereby affecting its expression levels. Notably, the overexpression of CXCL9 was found to partially attenuate the tumor-suppressive effects observed upon ALKBH5 knockdown. This observation suggested that CXCL9 functions as a downstream target of ALKBH5-mediated methylation, highlighting a novel mechanistic link between mRNA methylation and the regulation of chemokine expression in cancer biology.

The present study suggested that CXCL9 plays a dual role both in tumor progression and immune surveillance. On one hand, elevated levels of CXCL9 have been observed in CC tissues and correlate with advanced disease stage and tumor proliferation, invasion, metastasis and autophagy. On the other hand, CXCL9 has also been implicated in anti-tumor immunity within the CC microenvironment. Additionally, CXCL9 expression has been associated with improved overall survival and enhanced response to immunotherapy in CC patients, highlighting its potential as a predictive biomarker and therapeutic target. Furthermore, the dysregulation of CXCL9 in CC has been attributed to various molecular mechanisms, including m6a modifications. Understanding these underlying mechanisms may provide insights into the development of targeted therapies aimed at modulating CXCL9 expression and activity in CRC.

The present study has enhanced the understanding of ALKBH5-mediated modification of CXCL9 and its role in CRC, as well as its association with mitophagy. However, it has limitations. Although it analyzed the expression of CXCL9 across CRC stages using GEO and TCGA datasets, the absence of more comprehensive datasets restricted an in-depth understanding of its dynamic changes during disease progression. The expression of CXCL9 varies among different ethnicities and residual tumor classifications, which underscores the limitations of conducting experiments solely in cell lines. To address these gaps, it is hoped to collect additional patient samples in future experiments to confirm its role in CRC and explore its regulatory mechanisms on mitophagy at the *in vivo* level. The broader effect of CXCL9 on the tumor microenvironment and immune response will also be investigated to identify new therapeutic strategies for CRC. Further *in vivo* studies and clinical validations are essential for a complete understanding of the role of CXCL9 in tumor progression.

In conclusion, CXCL9 plays a multifaceted role in CRC pathogenesis, influencing both tumor progression and anti-tumor immunity. Further research is warranted to elucidate its precise mechanisms of action and explore its therapeutic potential in CRC management.

Acknowledgements

Not applicable.

Funding

The present study was supported by the 2024 Lincang City Association for Science and Technology Society Capacity Service Innovation and Development Project (grant no. 202404) and the Dali University Education Teaching Reform Project (grant no. JG09YX209).

Availability of data and materials

The data generated in the present study may be requested from the corresponding author.

Authors' contributions

GH was instrumental in the conceptualization and design of the study, led the analysis of bioinformatics data, was the primary author of the initial manuscript draft, and also coordinated revisions with all co-authors and provided comprehensive supervision and guidance throughout the project. SS was actively involved in the experimental procedures, data collection and preliminary data analysis, and also contributed to the writing of the manuscript and was responsible for securing partial funding for the research. MZ executed *in vitro* experiments using cell lines and played a significant role in the review of the manuscript. All authors read and approved the final manuscript.GH and SS confirm the authenticity of all the raw data.

Ethics approval and consent to participate

Not applicable.

Patient consent for publication

Not applicable.

Competing interests

The authors declare that they have no competing interests.

Authors' information

Geng Hu (https://orcid.org/0009-0008-7876-8139)
Shijun Shen (https://orcid.org/0000-0002-4532-9366)
Mingchao Zhu (https://orcid.org/0000-0001-5425-97803)

References

1. Morgan E, Arnold M, Gini A, Lorenzoni V, Cabasag CJ, Laversanne M, Vignat J, Ferlay J, Murphy N and Bray F: Global burden of colorectal cancer in 2020 and 2040: Incidence and mortality estimates from GLOBOCAN. Gut 72: 338-344, 2023.

2. Housini M, Dariya B, Ahmed N, Stevens A, Fiadjoe H, Nagaraju GP and Basha R: Colorectal cancer: Genetic alterations, novel biomarkers, current therapeutic strategies and clinical trials. Gene 892: 147857, 2024.
3. Potter JD, Slattery ML, Bostick RM and Gapstur SM: Colon cancer: A review of the epidemiology. Epidemiol Rev 15: 499-545, 1993.
4. Benson AB, Venook AP, Al-Hawary MM, Arain MA, Chen YJ, Ciombor KK, Cohen S, Cooper HS, Deming D, Farkas L, *et al*: Colon cancer, version 2.2021, NCCN clinical practice guidelines in oncology. J Natl Compr Canc Netw 19: 329-359, 2021.
5. Schlechter BL: Management of rectal cancer. Hematol Oncol Clin North Am 36: 521-537, 2022.
6. Schrag D, Shi Q, Weiser MR, Gollub MJ, Saltz LB, Musher BL, Goldberg J, Al Baghdadi T, Goodman KA, McWilliams RR, *et al*: Preoperative treatment of locally advanced rectal cancer. N Engl J Med 389: 322-334, 2023.
7. Niu SQ, Li RZ, Yuan Y, Xie WH, Wang QX, Chang H, Lu ZH, Ding PR, Li LR, Wu XJ, *et al*: Neoadjuvant chemoradiotherapy in patients with unresectable locally advanced sigmoid colon cancer: Clinical feasibility and outcome. Radiat Oncol 16: 93, 2021.
8. André T, Boni C, Mounedji-Boudiaf L, Navarro M, Tabernero J, Hickish T, Topham C, Zaninelli M, Clingan P, Bridgewater J, *et al*: Oxaliplatin, fluorouracil, and leucovorin as adjuvant treatment for colon cancer. N Engl J Med 350: 2343-2351, 2004.
9. André T, Shiu KK, Kim TW, Jensen BV, Jensen LH, Punt C, Smith D, Garcia-Carbonero R, Benavides M, Gibbs P, *et al*: Pembrolizumab in microsatellite-instability-high advanced colorectal cancer. N Engl J Med 383: 2207-2218, 2020.
10. Kong MY, Li LY, Lou YM, Chi HY and Wu JJ: Chinese herbal medicines for prevention and treatment of colorectal cancer: From molecular mechanisms to potential clinical applications. J Integr Med 18: 369-384, 2020.
11. Underwood PW, Ruff SM and Pawlik TM: Update on targeted therapy and immunotherapy for metastatic colorectal cancer. Cells 13: 245, 2024.
12. Cunningham D, Humblet Y, Siena S, Khayat D, Bleiberg H, Santoro A, Bets D, Mueser M, Harstrick A, Verslype C, *et al*: Cetuximab monotherapy and cetuximab plus irinotecan in irinotecan-refractory metastatic colorectal cancer. N Engl J Med 351: 337-345, 2004.
13. Chalabi M, Fanchi LF, Dijkstra KK, Van den Berg JG, Aalbers AG, Sikorska K, Lopez-Yurda M, Grootscholten C, Beets GL, Snaebjornsson P, *et al*: Neoadjuvant immunotherapy leads to pathological responses in MMR-proficient and MMR-deficient early-stage colon cancers. Nat Med 26: 566-576, 2020.
14. Ieranò C, Righelli D, D'Alterio C, Napolitano M, Portella L, Rea G, Auletta F, Santagata S, Trotta AM, Guardascione G, *et al*: In PD-1+ human colon cancer cells NIVOLUMAB promotes survival and could protect tumor cells from conventional therapies. J Immunother Cancer 10: e004032, 2022.
15. Suzuki S, Kawakami H, Miike T and Yamamoto S: Complete remission of colon cancer with ipilimumab monotherapy. Intern Med 60: 957-958, 2021.
16. Chalabi M, Verschoor YL, Tan PB, Balduzzi S, Van Lent AU, Grootscholten C, Dokter S, Büller NV, Grotenhuis BA, Kuhlmann K, *et al*: Neoadjuvant immunotherapy in locally advanced mismatch repair-deficient colon cancer. N Engl J Med 390: 1949-1958, 2024.
17. Zhou C, Gao Y, Ding P, Wu T and Ji G: The role of CXCL family members in different diseases. Cell Death Discov 9: 212, 2023.
18. Cambier S, Gouwy M and Proost P: The chemokines CXCL8 and CXCL12: Molecular and functional properties, role in disease and efforts towards pharmacological intervention. Cell Mol Immunol 20: 217-251, 2023.
19. House IG, Savas P, Lai J, Chen AXY, Oliver AJ, Teo ZL, Todd KL, Henderson MA, Giuffrida L, Petley EV, *et al*: Macrophage-derived CXCL9 and CXCL10 are required for antitumor immune responses following immune checkpoint blockade. Clin Cancer Res 26: 487-504, 2020.
20. Mikucki ME, Fisher DT, Matsuzaki J, Skitzki JJ, Gaulin NB, Muhitch JB, Ku AW, Frelinger JG, Odunsi K, Gajewski TF, *et al*: Non-redundant requirement for CXCR3 signalling during tumoricidal T-cell trafficking across tumour vascular checkpoints. Nat Commun 6: 7458, 2015.
21. Tokunaga R, Zhang W, Naseem M, Puccini A, Berger MD, Soni S, McSkane M, Baba H and Lenz HJ: CXCL9, CXCL10, CXCL11/CXCR3 axis for immune activation-A target for novel cancer therapy. Cancer Treat Rev 63: 40-47, 2018.
22. Andersson As, Yang SC, Huang M, Zhu L, Kar UK, Batra RK, Elashoff D, Strieter RM, Dubinett SM and Sharma S: IL-7 promotes CXCR3 ligand-dependent T cell antitumor reactivity in lung cancer. J Immunol 182: 6951-6958, 2009.
23. Wu L, Sun S, Qu F, Sun M, Liu X, Sun Q, Cheng L, Zheng Y and Su G: CXCL9 influences the tumor immune microenvironment by stimulating JAK/STAT pathway in triple-negative breast cancer. Cancer Immunol Immunother 72: 1479-1492, 2023.
24. Santana-Hernández S, Suarez-Olmos J, Servitja S, Berenguer-Molins P, Costa-Garcia M, Comerma L, Rea A, Perera-Bel J, Menendez S, Arpí O, *et al*: NK cell-triggered CCL5/IFNγ-CXCL9/10 axis underlies the clinical efficacy of neoadjuvant anti-HER2 antibodies in breast cancer. J Exp Clin Cancer Res 43: 10, 2024.
25. Bronger H, Karge A, Dreyer T, Zech D, Kraeft S, Avril S, Kiechle M and Schmitt M: Induction of cathepsin B by the CXCR3 chemokines CXCL9 and CXCL10 in human breast cancer cells. Oncol Lett 13: 4224-4230, 2017.
26. Wang J, Wang Q, Guan Y, Sun Y, Wang X, Lively K, Wang Y, Luo M, Kim JA, Murphy EA, *et al*: Breast cancer cell-derived microRNA-155 suppresses tumor progression via enhancing immune cell recruitment and antitumor function. J Clin Invest 132: e157248, 2022.
27. Romano G, Paradiso F, Li P, Shukla P, Barger LN, El Naggar O, Miller JP, Liang RJ, Helms TL, Lazar AJ, *et al*: Microparticle-delivered Cxcl9 prolongs braf inhibitor efficacy in melanoma. Cancer Immunol Res 11: 558-569, 2023.
28. Cui Y, Miao Y, Cao L, Guo L, Cui Y, Yan C, Zeng Z, Xu M and Han T: Activation of melanocortin-1 receptor signaling in melanoma cells impairs T cell infiltration to dampen antitumor immunity. Nat Commun 14: 5740, 2023.
29. Lim RJ, Salehi-Rad R, Tran LM, Oh MS, Dumitras C, Crosson WP, Li R, Patel TS, Man S, Yean CE, *et al*: CXCL9/10-engineered dendritic cells promote T cell activation and enhance immune checkpoint blockade for lung cancer. Cell Rep Med 5: 101479, 2024.
30. Woo SJ, Kim Y, Kang HJ, Jung H, Youn DH, Hong Y, Lee JJ and Hong JY: Tuberculous pleural effusion-induced Arg-1^{+} macrophage polarization contributes to lung cancer progression via autophagy signaling. Respir Res 25: 198, 2024.
31. Shannon P, Markiel A, Ozier O, Baliga NS, Wang JT, Ramage D, Amin N, Schwikowski B and Ideker T: Cytoscape: A software environment for integrated models of biomolecular interaction networks. Genome Res 13: 2498-2504, 2003.
32. Assenov Y, Ramírez F, Schelhorn SE, Lengauer T and Albrecht M: Computing topological parameters of biological networks. Bioinformatics 24: 282-284, 2008.
33. Győrffy B: Integrated analysis of public datasets for the discovery and validation of survival-associated genes in solid tumors. Innovation (Camb) 5: 100625, 2024.
34. Ru B, Wong CN, Tong Y, Zhong JY, Zhong SSW, Wu WC, Chu KC, Wong CY, Lau CY, Chen I, *et al*: TISIDB: An integrated repository portal for tumor-immune system interactions. Bioinformatics 35: 4200-4202, 2019.
35. Zhou Y, Zeng P, Li YH, Zhang Z and Cui Q: SRAMP: Prediction of mammalian N6-methyladenosine (m6A) sites based on sequence-derived features. Nucleic Acids Res 44: e91, 2016.
36. Livak KJ and Schmittgen TD: Analysis of relative gene expression data using real-time quantitative PCR and the 2(-Delta Delta C(T)) method. Methods 25: 402-408, 2001.
37. Luo X, Tai J, Zhao Y, Zhao P, Sun D and Wang L: Associations of C-X-C motif chemokine ligands 1/2/8/13/14 with clinicopathological features and survival profile in patients with colorectal cancer. Oncol Lett 24: 348, 2022.
38. Zhuo C, Ruan Q, Zhao X, Shen Y and Lin R: CXCL1 promotes colon cancer progression through activation of NF-κB/P300 signaling pathway. Biol Direct 17: 34, 2022.
39. Lepsenyi M, Algethami N, Al-Haidari AA, Algaber A, Syk I, Rahman M and Thorlacius H: CXCL2-CXCR2 axis mediates αV integrin-dependent peritoneal metastasis of colon cancer cells. Clin Exp Metastasis 38: 401-410, 2021.
40. Han B, Feng D, Yu X, Liu Y, Yang M, Luo F, Zhou L and Liu F: MicroRNA-144 mediates chronic inflammation and tumorigenesis in colorectal cancer progression via regulating C-X-C motif chemokine ligand 11. Exp Ther Med 16: 1935-1943, 2018.
41. Cao Y, Jiao N, Sun T, Ma Y, Zhang X, Chen H, Hong J and Zhang Y: CXCL11 correlates with antitumor immunity and an improved prognosis in colon cancer. Front Cell Dev Biol 9: 646252, 2021.

42. Li X, Lu M, Yuan M, Ye J, Zhang W, Xu L, Wu X, Hui B, Yang Y, Wei B, *et al*: CXCL10-armed oncolytic adenovirus promotes tumor-infiltrating T-cell chemotaxis to enhance anti-PD-1 therapy. Oncoimmunology 11: 2118210, 2022.
43. Wang B, Wang M, Ao D and Wei X: CXCL13-CXCR5 axis: Regulation in inflammatory diseases and cancer. Biochim Biophys Acta Rev Cancer 1877: 188799, 2022.
44. Hussain M, Liu J, Wang GZ and Zhou GB: CXCL13 signaling in the tumor microenvironment. Adv Exp Med Biol 1302: 71-90, 2021.
45. Liu G, Sun J, Yang ZF, Zhou C, Zhou PY, Guan RY, Sun BY, Wang ZT, Zhou J, Fan J, *et al*: Cancer-associated fibroblast-derived CXCL11 modulates hepatocellular carcinoma cell migration and tumor metastasis through the circUBAP2/miR-4756/IFIT1/3 axis. Cell Death Dis 12: 260, 2021.
46. Wang J, Ouyang X, Zhu W, Yi Q and Zhong J: The Role of CXCL11 and its receptors in cancer: Prospective but challenging clinical targets. Cancer Control 31: 10732748241241162, 2024.
47. Wu X, Sun A, Yu W, Hong C and Liu Z: CXCL10 mediates breast cancer tamoxifen resistance and promotes estrogen-dependent and independent proliferation. Mol Cell Endocrinol 512: 110866, 2020.
48. Zuo H and Wan Y: Inhibition of myeloid PD-L1 suppresses osteoclastogenesis and cancer bone metastasis. Cancer Gene Ther 29: 1342-1354, 2022.
49. Han Y, Liu D and Li L: PD-1/PD-L1 pathway: Current researches in cancer. Am J Cancer Res 10: 727-742, 2020.
50. Zhang Z, Zhang H, Cui L, Wang X, Wang D, Liu Z, Zhang X and Tang Z: An MMAE-loaded PDL1 active targeting nanomedicine for the precision treatment of colon cancer. Biomater Sci 11: 5195-5204, 2023.
51. Wang S, Song Y, Cao K, Zhang L, Fang X, Chen F, Feng S and Yan F: Photothermal therapy mediated by gold nanocages composed of anti-PDL1 and galunisertib for improved synergistic immunotherapy in colorectal cancer. Acta Biomater 134: 621-632, 2021.
52. Gao Y, Zhao K, Huang Y, Zhang D, Luo N, Peng X, Yang F, Xiao W, Wang M, Shi R and Miao H: Lanosterol synthase deficiency promotes tumor progression by orchestrating PDL1-dependent tumor immunosuppressive microenvironment. MedComm (2020) 5: e528, 2024.
53. Limagne E and Ghiringhelli F: Mitophagy: A new actor in the efficacy of chemo-immunotherapy. Autophagy 18: 3033-3034, 2022.
54. Wang T, Gao T, Fujisawa M, Ohara T, Sakaguchi M, Yoshimura T and Matsukawa A: SPRED2 is a novel regulator of autophagy in hepatocellular carcinoma cells and normal hepatocytes. Int J Mol Sci 25: 6269, 2024.
55. Guido C, Whitaker-Menezes D, Lin Z, Pestell RG, Howell A, Zimmers TA, Casimiro MC, Aquila S, Ando' S, Martinez-Outschoorn UE, *et al*: Mitochondrial fission induces glycolytic reprogramming in cancer-associated myofibroblasts, driving stromal lactate production, and early tumor growth. Oncotarget 3: 798-810, 2012.
56. Qiu Y, Wang J, Li H, Yang B, Wang J, He Q and Weng Q: Emerging views of OPTN (optineurin) function in the autophagic process associated with disease. Autophagy 18: 73-85, 2022.
57. Liu X, Li P, Huang Y, Li H, Liu X, Du Y, Lin X, Chen D, Liu H and Zhou Y: M^6A demethylase ALKBH5 regulates FOXO1 mRNA stability and chemoresistance in triple-negative breast cancer. Redox Biol 69: 102993, 2024.
58. Liu M and Chen X: N6-methyladenosine demethylase ALKBH5 promotes pyroptosis by modulating PTBP1 mRNA stability in LPS-induced myocardial dysfunction. Acta Cardiol Sin 40: 312-321, 2024.
59. Wang YY, Ye LH, Zhao AQ, Gao WR, Dai N, Yin Y and Zhang X: M6A modification regulates tumor suppressor DIRAS1 expression in cervical cancer cells. Cancer Biol Ther 25: 2306674, 2024.